

# Nonvolatile spin field effect transistor based on $\text{VSi}_2\text{N}_4/\text{Sc}_2\text{CO}_2$ multiferroic heterostructure

Xian Zhang,<sup>1</sup> Bang Liu,<sup>2</sup> Junsheng Huang,<sup>2</sup> Xinwei Cao,<sup>1</sup> Yunzhe Zhang,<sup>1</sup> and Zhi-Xin Guo<sup>2,\*</sup>

<sup>1</sup>College of Mechanical and Materials Engineering, Xi'an University, Xi'an 710065, China

<sup>2</sup>State Key Laboratory for Mechanical Behavior of Materials and School of Materials Science and Engineering, Xi'an Jiaotong University, Xi'an, Shaanxi, 710049, China

(Dated: November 8, 2023)

We report first-principles calculations that propose a nonvolatile spin field effect transistor (spin-FET) based on a van der Waals multiferroic heterostructure, i.e.,  $\text{VSi}_2\text{N}_4/\text{Sc}_2\text{CO}_2$ . We find that the inversion of ferroelectric polarization of monolayer  $\text{Sc}_2\text{CO}_2$  can efficiently modulate the electronic states of monolayer  $\text{VSi}_2\text{N}_4$ . A half-metal to half-semiconductor phase transition of  $\text{VSi}_2\text{N}_4$  can be efficiently realized, which leads to distinct electronic transport properties. We additionally construct a spin-FET device based on the multiferroic heterostructure. We find that the  $\text{VSi}_2\text{N}_4/\text{Sc}_2\text{CO}_2$  based Spin-FET has remarkable all-electric-controlled performance. A large on-off current ratio of about 650% induced by the inversion of  $\text{Sc}_2\text{CO}_2$  ferroelectric polarization can be obtained under a small bias voltage (0.02 V). We also find an interesting spatially-separated spin-polarized transport phenomenon, with the pure spin-up (spin-down) electrons transporting merely in  $\text{VSi}_2\text{N}_4$  ( $\text{Sc}_2\text{CO}_2$ ). Our study provides a promising approach for constructing low-energy-dissipation and nonvolatile FET devices.

## I. INTRODUCTION

During the continuous miniaturization of electronic products, Joule heating and quantum limit on device becomes the bottlenecks that prevent further increase operation speed and information density, which invalidate the Moore's law<sup>1,2</sup>. Spintronics is believed to be the strong candidate of the future technology in the post Si-era<sup>3,4</sup>. For any operation in spintronics, the techniques for injection, detection, manipulation, transport, and storage of spins need to be established<sup>5</sup>. In spin-based devices, encoding and reading out spin information in single spins can be considered the ultimate limit for scaling magnetic information. Spin field-effect transistor (spin-FET) is a fundamental spin-based device for the spin operation<sup>6,7</sup>. Developing low-power cost spin-FET that can efficiently realize the *on* or *off* state of single spin current is crucial for the development of spintronics<sup>8</sup>.

Traditionally, spin-FET is a three terminal device with spin polarized current flowing between drain and source terminals and the gate terminal is used to control this current. As proposed by Datta and Das, the spin precession motion of electron can be controlled through the Rashba spin-orbit coupling effect, where *on* and *off* states are distinguished by  $\pi$  phase difference in spin precession motion<sup>6,7</sup>. Nonetheless, since the realization of  $\pi$  phase difference in the spin-FETs depends on the precise control of gate voltage, such spin-FET device meets challenge of the nonvolatile functionality, which is usually realized by using a ferroelectric material as gating.

In this work, based on the first-principles calculations, we propose a spin-FET possessing remarkable nonvolatile *on* and *off* functionality. Such spin-FET uses a two-dimensional (2D) van der Waals (vdW) multiferroic heterostructure (e.g. composed by monolayer  $\text{VSi}_2\text{N}_4$  and monolayer  $\text{Sc}_2\text{CO}_2$ ) as the channel material, instead of the nonmagnetic semiconductors (like

InAs, InAlAs, etc.) that are generally adopted in traditional spin-FET devices<sup>9</sup>. In the multiferroic heterostructure, ferromagnetic material  $\text{VSi}_2\text{N}_4$  has a half-semiconductor characteristic and is mainly responsible for the spin transport<sup>10,11</sup>. Whereas, the ferroelectric material  $\text{Sc}_2\text{CO}_2$  has a semiconductor characteristic<sup>12,13</sup> and is mainly in charge of controlling the spin-polarized electronic structure of  $\text{VSi}_2\text{N}_4$ . It is found that the inversion of ferroelectric polarization of  $\text{Sc}_2\text{CO}_2$  can efficiently change the spin-up electronic structure of  $\text{VSi}_2\text{N}_4$ , leading to a half-semiconductor to half-metal transition. It is also found that the  $\text{VSi}_2\text{N}_4/\text{Sc}_2\text{CO}_2$  based Spin-FET has remarkable all-electric-controlled performance, where a large on-off current ratio can be obtained under a small bias voltage. Additionally, an interesting spatially-separated spin-polarized transport phenomenon, with the pure spin-up (spin-down) electrons transporting merely in  $\text{VSi}_2\text{N}_4$  ( $\text{Sc}_2\text{CO}_2$ ), is observed.

## II. METHOD

Geometric optimization and electronic structures of the heterostructure are calculated by density-functional theory (DFT) with the projector-augmented-wave (PAW) method, which is implemented in the Vienna ab initio simulation package<sup>14,15</sup>. The exchange-correlation interaction is treated by the generalized gradient approximation (GGA) based on the Perdew-Burke-Ernzerhof (PBE) function and HSE06 functional for the geometric optimization and electronic structures, respectively<sup>16,17</sup>. The convergence standards of the atomic energy and positions are less than  $1 \times 10^{-5}$  eV per atom and  $1 \times 10^{-2}$  eV  $\text{\AA}^{-1}$ , respectively. The cutoff energy of wave function is set to 500 eV. The Brillouin zone (BZ) is sampled by a  $9 \times 9 \times 1$  Monkhorst-Pack k-point mesh.

The transport properties are simulated based on the DFT method combined with the nonequilibrium Green's function (NEGF) formalism, using the Atomistix ToolKit (ATK) 2019 package<sup>18</sup>. In the calculations, the Tier 3 basis set of the linear combination of atomic orbital (LCAO) is adopted with Hartwigsen-Goedecker-Hutter pseudopotentials and GGA in the form of the PBE function is utilized to represent the exchange and correlation interactions. The transmission calculations are carried out with the PBE pseudopotentials distributed in the Quantum-Wise package<sup>18,19</sup>. A density mesh-cutoff of 75 Hartree is employed, and the BZ is sampled using a  $6 \times 1 \times 94$  k-point grid in the transport calculations. At a bias-voltage  $V_b$ , the spin-resolved current ( $I_\sigma$ ) can be calculated as follows:

$$I_\sigma(V_b) = \frac{e}{h} \int_{-\infty}^{+\infty} dE [f(E, \mu_L) - f(E, \mu_R)] T_\sigma(E, V_b), \quad (1)$$

where  $f(E, \mu_L)$  and  $f(E, \mu_R)$  are the Fermi-Dirac distribution of the left and right electrodes, respectively.  $\mu_L$  and  $\mu_R$  are the electrochemical potentials of the left and right electrodes, respectively, and  $T_\sigma(E)$  is the transmission probability for an electron at energy  $E$  with spin  $\sigma$ . Note that the linear response current originated from the equilibrium transmission spectrum at zero bias is considered in the calculations<sup>20</sup>.

### III. RESULTS

The heterostructure is constructed by a ferromagnetic (FM) monolayer  $\text{VSi}_2\text{N}_4$  and a ferroelectric monolayer  $\text{Sc}_2\text{CO}_2$ . The monolayer  $\text{Sc}_2\text{CO}_2$  was predicted to have a sizable out-of-plane electrical polarization as high as  $1.60 \mu\text{C}/\text{cm}^3$ , and the reverse of electric polarization is achieved via displacement of C atoms with an energy barrier about  $0.52 \text{ eV}$ <sup>12</sup>. The  $\text{Sc}_2\text{CO}_2$  with carbon-up and carbon-down configurations correspond to the polarization-up ( $\text{P}\uparrow$ ) and polarization-down states ( $\text{P}\downarrow$ ), respectively (see Fig. 1(a)). On the other hand,  $\text{VSi}_2\text{N}_4$  is a theoretically predicted 2D magnetic material, which is a member of the  $\text{MA}_2\text{Z}_4$  family. The Curie temperature of monolayer  $\text{VSi}_2\text{N}_4$  is predicted to be higher than room temperature, showing the promising potential applications in future spintronic devices<sup>10</sup>. Fig. 1(b) further shows the calculated band structure of monolayer  $\text{VSi}_2\text{N}_4$ . An interesting characteristic is that there is only spin-up electrons in a wide energy range around the Fermi energy ( $E_F$ ), i.e.,  $[-1.7, 1.4] \text{ eV}$ , making  $\text{VSi}_2\text{N}_4$  an ideal half-semiconductor.

Considering that the in-plane lattice constant of free-standing  $\text{Sc}_2\text{CO}_2$  and  $\text{VSi}_2\text{N}_4$  are  $5.74 \text{ \AA}$  and  $2.88 \text{ \AA}$ , respectively, a  $2 \times 2$  super-periodicity of  $\text{VSi}_2\text{N}_4$  is commensurate to the  $1 \times 1$   $\text{Sc}_2\text{CO}_2$ , with a lattice mismatch is of 1.23%. As shown in Fig. S1, we have considered three typical stacking configurations of the  $\text{VSi}_2\text{N}_4/\text{Sc}_2\text{CO}_2$  heterostructure, namely, hollow configuration, bridge configuration, and top configuration. The

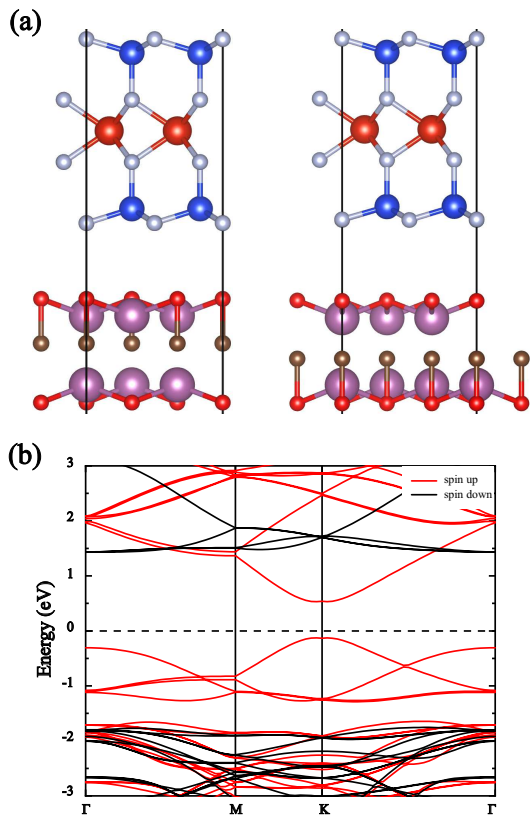


FIG. 1. Atomic structures of  $\text{VSi}_2\text{N}_4/\text{Sc}_2\text{CO}_2$  heterostructure with  $\text{Sc}_2\text{CO}_2$  in  $\text{P}\uparrow$  and  $\text{P}\downarrow$  polarizations and the spin-resolved energy bands of  $\text{VSi}_2\text{N}_4$ . (a) Atomic structures of  $\text{VSi}_2\text{N}_4/\text{Sc}_2\text{CO}_2$  heterostructure, with  $\text{Sc}_2\text{CO}_2$  in  $\text{P}\uparrow$  (left panel) polarization and  $\text{P}\downarrow$  (right panel) polarizations, respectively. (b) Band structure of  $\text{VSi}_2\text{N}_4$ . The grey, large red, and blue balls represent the N, Si, and V atoms, respectively. The red, big purple, and orange balls represent the O, Sc, and C atoms, respectively.

calculated total energies of the three configurations are  $-300.77698 \text{ eV}$ ,  $-300.77690$ , and  $-300.77688 \text{ eV}$ , respectively, showing that the hollow configuration (also see Fig. 1(a)) is the most stable. Nevertheless, the total energy difference among the three configurations is very small ( $\leq 0.1 \text{ meV}$ ). This feature indicates that all the three configurations can be obtained in experiments. Moreover, it is found that the interlayer spacing between  $\text{VSi}_2\text{N}_4$  and  $\text{Sc}_2\text{CO}_2$  is  $3.06 \text{ \AA}$  and  $2.82 \text{ \AA}$  for the  $\text{P}\uparrow$  and  $\text{P}\downarrow$  polarization states, respectively. It is known that the atomic radii of O and N atoms, which are located at the surface of  $\text{Sc}_2\text{CO}_2$  and  $\text{VSi}_2\text{N}_4$ , respectively, are  $0.66 \text{ \AA}$  and  $0.71 \text{ \AA}$ . Hence, the sum of their atomic radii is much smaller than the interlayer spacing, showing the nature of vdW interaction between  $\text{Sc}_2\text{CO}_2$  and  $\text{VSi}_2\text{N}_4$ . To ensure that the  $\text{VSi}_2\text{N}_4/\text{Sc}_2\text{CO}_2$  heterostructure is energetically stable, we further calculate the binding energy ( $E_b$ ) between  $\text{VSi}_2\text{N}_4$  and  $\text{Sc}_2\text{CO}_2$ , which is defined as  $E_b = (E_S + E_V - E_{tot})/N$ . Here  $E_S$ ,  $E_V$ , and

$E_{tot}$  are the total energy of monolayer  $\text{Sc}_2\text{CO}_2$ , monolayer  $\text{VSi}_2\text{N}_4$ , and the  $\text{VSi}_2\text{N}_4/\text{Sc}_2\text{CO}_2$  heterostructure, respectively.  $N$  represents the number of O atoms located at the interface of the heterostructure. In the hollow configuration, it is found that  $E_b = -31 \text{ meV}/\text{\AA}^2$  and  $-21 \text{ meV}/\text{\AA}^2$  for the  $\text{P}\uparrow$  and  $\text{P}\downarrow$  polarization states, respectively. This result shows that the heterostructure is energetically stable under a vdW interlayer interaction.

Then, we discuss the electronic properties of  $\text{VSi}_2\text{N}_4$  manipulated by the polarization of  $\text{Sc}_2\text{CO}_2$ . In comparison with the band structure of freestanding  $\text{VSi}_2\text{N}_4$  (Fig. 1(b)), there is an obvious upshift of  $E_F$  of  $\text{VSi}_2\text{N}_4$  in the heterostructure in the  $\text{P}\uparrow$  polarization state (Figs. 2(a) and 2(b)). As a result, an half-semiconductor to half-metal transition occurs in  $\text{VSi}_2\text{N}_4$  under the effect of  $\text{Sc}_2\text{CO}_2$ . Moreover, the band gap of spin-up electrons remarkably decreases from 0.7 eV to 0.1 eV, showing the strong interface effect on the electronic structure of  $\text{VSi}_2\text{N}_4$ . It is noticed that the spin-up energy bands in the heterostructure present a type-III band alignment, whereas the spin-down energy bands have a type-II band alignment. This feature indicates that there is an obvious electron transfer from  $\text{Sc}_2\text{CO}_2$  to  $\text{VSi}_2\text{N}_4$ , which fills up the spin-up conduction states. As for the case of  $\text{P}\downarrow$  polarization state, the spin-up energy bands of  $\text{VSi}_2\text{N}_4$  present a type-I band alignment, and the spin-down energy bands form a type-II band alignment (Figs. 2(c) and 2(d)). This result shows that there is little charge transfer between  $\text{Sc}_2\text{CO}_2$  and  $\text{VSi}_2\text{N}_4$ . In comparison with that of freestanding  $\text{VSi}_2\text{N}_4$ , there is also a sizable decrease of band gap of the spin-up electrons (from 0.7 eV to 0.2 eV), whereas the band gap of spin-down electrons changes little. This result is similar to that of the  $\text{P}\uparrow$  polarization state. It is noticed that the  $E_F$  lies in the band gap of spin-up electrons, which makes the heterostructure a half-semiconductor. The above results show that the inversion of out-of-plane polarization of the  $\text{Sc}_2\text{CO}_2$  can dramatically change the band alignment as well as the band structure of  $\text{VSi}_2\text{N}_4$  in the heterostructure.

To further show the  $\text{Sc}_2\text{CO}_2$  polarization dependent charge transfer effect on band structure of  $\text{VSi}_2\text{N}_4$ , we calculate the electron density difference (EDF) of  $\text{VSi}_2\text{N}_4/\text{Sc}_2\text{CO}_2$  heterostructure. As shown in Fig. 3(a), there are extra electron (hole) in the  $\text{VSi}_2\text{N}_4$  ( $\text{Sc}_2\text{CO}_2$ ) part of the  $\text{P}\uparrow$  configuration, compared with that of the freestanding  $\text{VSi}_2\text{N}_4$  ( $\text{Sc}_2\text{CO}_2$ ). According to Bader's charge analysis, around 0.26 electron transfers from  $\text{Sc}_2\text{CO}_2$  to  $\text{VSi}_2\text{N}_4$ , which results in the half-semiconductor to half-metal transition of  $\text{VSi}_2\text{N}_4$ . On the other hand, we do not observe any significant charge transfer from  $\text{Sc}_2\text{CO}_2$  to  $\text{VSi}_2\text{N}_4$  in the  $\text{P}\downarrow$  configuration (see Fig. 3(b)). Hence,  $\text{VSi}_2\text{N}_4$  holds the half-semiconductor characteristic. This result agrees well with the  $\text{Sc}_2\text{CO}_2$ -polarization dependent band alignments in the heterostructure.

In addition, the band projection analysis (Fig. S2) shows that both the conduction band minimum (CBM) and valence band maximum (VBM) of spin-up electronic

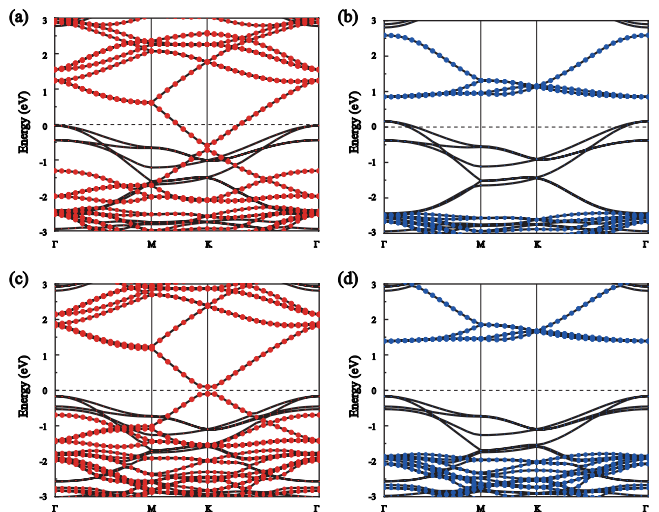


FIG. 2. Spin-resolved energy bands of  $\text{VSi}_2\text{N}_4/\text{Sc}_2\text{CO}_2$  heterostructure with  $\text{Sc}_2\text{CO}_2$  in  $\text{P}\uparrow$  (a,b) and  $\text{P}\downarrow$  (c,d) polarizations. (a) and (c) are the energy bands of spin-up electrons, (b) and (d) are the energy bands of spin-down electrons. Red and blue symbols denote spin-up and spin-down electronic states of  $\text{VSi}_2\text{N}_4$ , respectively.

states of  $\text{VSi}_2\text{N}_4$  are attributed to the  $d_z^2$  and  $d_{x^2-y^2}$  (eg orbitals of V atoms), which locate in the center of  $\text{VSi}_2\text{N}_4$ . Note that the eg orbitals of V atoms also give rise to the CBM of spin-down electrons as shown in Fig. S2, and thus induce the type-II band alignment. This result shows that the atomic layer composed of V atoms is mainly responsible to the spin current transport in the  $\text{VSi}_2\text{N}_4/\text{Sc}_2\text{CO}_2$  heterostructure.

Next, we discuss the plentiful nonvolatile spin transport properties of  $\text{VSi}_2\text{N}_4$  induced by the  $\text{Sc}_2\text{CO}_2$  polarizations. We first propose a novel spin-FET structure based on the  $\text{VSi}_2\text{N}_4/\text{Sc}_2\text{CO}_2$  heterostructure, as shown in Fig. 3(a). In this structure, one can effectively control the inversion of  $\text{Sc}_2\text{CO}_2$  ferroelectric polarization by a bottom gate. When  $\text{Sc}_2\text{CO}_2$  is in  $\text{P}\uparrow$  polarization, according to the band structure of  $\text{VSi}_2\text{N}_4/\text{Sc}_2\text{CO}_2$  shown in Fig. 2(a), one expects a large spin-up current and thus the spin-FET is in an *on* state, due to the half-metal characteristic of  $\text{VSi}_2\text{N}_4$ . In contrast, when  $\text{Sc}_2\text{CO}_2$  is in  $\text{P}\downarrow$  polarization, a small spin-up current and thus the *off* state is expected within a low bias voltage region, owing to the half-semiconductor characteristic of  $\text{VSi}_2\text{N}_4$  (Figs. 2(c)). Note that, there is no spin-down current from  $\text{VSi}_2\text{N}_4$ , due to the large band gap of the spin-down electrons of  $\text{VSi}_2\text{N}_4$  (Figs. 2(b) and 2(d)). Consequently, a pure spin-polarized current can be realized in the  $\text{VSi}_2\text{N}_4/\text{Sc}_2\text{CO}_2$  based nonvolatile spin-FET.

To verify above argument, we further calculate the electronic transport property of the spin-FET. Figs. 4(b) and 4(c) show the transmission spectrum of this device at zero bias with  $\text{Sc}_2\text{CO}_2$  in  $\text{P}\uparrow$  and  $\text{P}\downarrow$  polarizations, respectively. It is seen that the transmission of spin-up

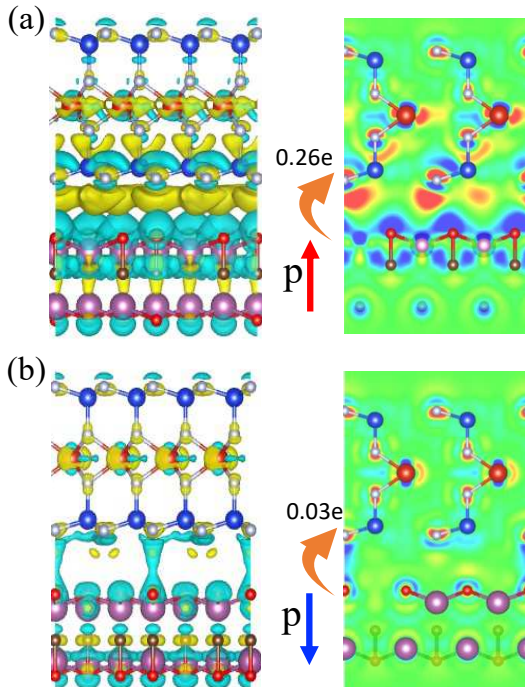


FIG. 3. Electron density difference (EDF) of  $\text{VSi}_2\text{N}_4/\text{Sc}_2\text{CO}_2$  heterostructure. (a) EDF with  $\text{Sc}_2\text{CO}_2$  in  $\text{P}\uparrow$  polarization. (b) EDF with  $\text{Sc}_2\text{CO}_2$  in  $\text{P}\downarrow$  polarization. The left panels in (a) and (b) are the isosurface of EDF, where the yellow and azure colors represent the positive and negative values, respectively. The right panels in (a) and (b) are the contour plots of EDF, where the red and blue colors correspond to the normalized maximum of the positive and negative values, respectively.

electrons in  $\text{P}\uparrow$  condition reaches up to 1.4 at Fermi level, where as it is only 0.1 in the  $\text{P}\downarrow$  polarization state. The nonzero transmission at Fermi level in the  $\text{P}\downarrow$  polarization state can be attributed to the room temperature adopted in this study, which induces the broadening of band structure. As a result, an on-off ratio of 14 for the spin-up electrons of  $\text{VSi}_2\text{N}_4$  can be obtained in the low bias voltage region. Notably, in the  $\text{P}\uparrow$  polarization state, there is also sizable transmission at Fermi level (0.7) for the spin-down electrons, which comes entirely from  $\text{Sc}_2\text{CO}_2$  (as shown in Fig. 2(b), the VBM of spin-down electrons of  $\text{Sc}_2\text{CO}_2$  upshifts to 0.2 eV above  $E_F$ ). This result shows an interesting spatially-separated spin-polarized transport phenomenon in the spin-FET, which is expected to have potential applications in the future spintronics. Note that the transmission of spin-down electrons of both  $\text{VSi}_2\text{N}_4$  and  $\text{Sc}_2\text{CO}_2$  in the spin-FET goes to zero at higher energy levels, i.e.,  $E \geq 0.15$  eV and 0.01 eV with  $\text{Sc}_2\text{CO}_2$  in  $\text{P}\uparrow$  and  $\text{P}\downarrow$  polarizations, respectively. In this condition, the spin-down current from  $\text{Sc}_2\text{CO}_2$  can be completely inhibited, and thus the pure spin-up current transport can be realized. This result implies the good spin-valve performance of the  $\text{VSi}_2\text{N}_4/\text{Sc}_2\text{CO}_2$  based devices.

Finally, we discuss the on-off ratio of the total current

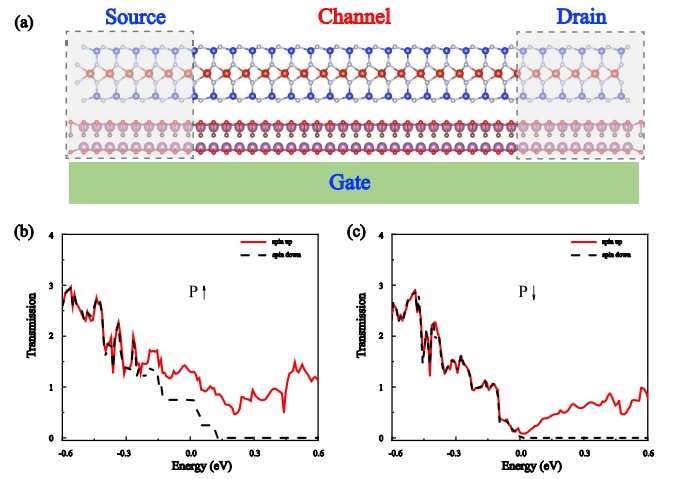


FIG. 4. (a) The schematic structure of the proposed spin-FET based on the  $\text{VSi}_2\text{N}_4/\text{Sc}_2\text{CO}_2$  heterostructure. (b) The calculated spin-polarized transmission spectrum of the spin-FET with  $\text{Sc}_2\text{CO}_2$  in  $\text{P}\uparrow$  polarization. (c) The calculated spin-polarized transmission spectrum of the spin-FET with  $\text{Sc}_2\text{CO}_2$  in  $\text{P}\downarrow$  polarization.

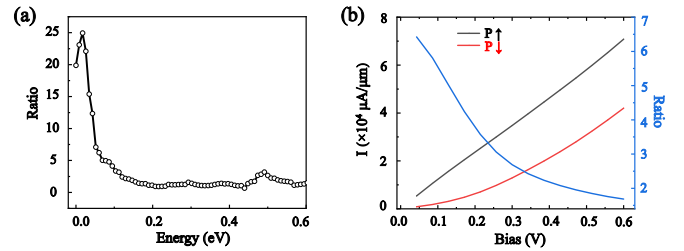


FIG. 5. (a) The ratio of total transmission (sum of spin-up and spin-down transmission) between the  $\text{P}\uparrow$  and  $\text{P}\downarrow$  polarization states. (b) The calculated I-V curves of the total current (sum of spin-up and spin-down current) with  $\text{Sc}_2\text{CO}_2$  in  $\text{P}\uparrow$  (solid red line) and  $\text{P}\downarrow$  (solid black line) polarizations, respectively. The blue line in (b) shows the on-off ratio of total current.

in the spin-FET. Fig. 5(a) shows the on-off ratio of the total transmission (sum of spin-up and spin-down transmissions). It is seen that the on-off ratio monotonically increases with decreasing the bias voltage from 0.6 V, reaching 2500% around the Fermi level. This result indicates that a drastic total current (sum of spin-up and spin-down currents) difference can be induced by the inversion of ferroelectric polarizations of  $\text{Sc}_2\text{CO}_2$  in the low bias voltage region. Fig. 5(b) further shows the calculated I-V curves of the total current in  $\text{P}\uparrow$  and  $\text{P}\downarrow$  polarization states, respectively. In the  $\text{P}\uparrow$  state, the total current linearly increases with the bias voltage. Whereas, in the  $\text{P}\downarrow$  state it quadratically increases with the bias voltage. As a result, the on-off ratio of total current monotonically increases with decreasing the voltage, and a large on-off ratio of about 650% can be obtained when

a small bias voltage (0.02 V) is applied (Fig. 5(b)).

#### IV. SUMMARY

In summary, based on the  $\text{VSi}_2\text{N}_4/\text{Sc}_2\text{CO}_2$  multiferroic heterostructure, we propose a way of realizing nonvolatile spin-FET, which has a low-energy-consumption characteristic. The DFT calculations show that the inversion of  $\text{Sc}_2\text{CO}_2$  ferroelectric polarization can efficiently modulate the spin-polarized electronic structure of  $\text{VSi}_2\text{N}_4$ , which induces a half metal to half-semiconductor transition. Such electronic phase transition can lead to significant change of electronic transport properties, which is an essential concept of the nonvolatile spin-FET. We additionally construct a spin-FET structure based on the  $\text{VSi}_2\text{N}_4/\text{Sc}_2\text{CO}_2$  heterostructure. The electronic transport calculations show that the Spin-FET has remarkable all-electric-controlled performance, where a large on-off

ratio (about 650%) of the total current has been obtained when a small bias voltage (0.02 V) is applied. Moreover, an interesting spatially-separated spin-polarized transport phenomenon has been observed when  $\text{Sc}_2\text{CO}_2$  is in  $P\uparrow$  polarization, where the pure spin-up (spin-down) electrons transport in  $\text{VSi}_2\text{N}_4$  ( $\text{Sc}_2\text{CO}_2$ ). These findings can be helpful to the design of high-performance nonvolatile 2D Spin-FET devices.

#### ACKNOWLEDGMENTS

We acknowledge financial support from the Ministry of Science and Technology of the People's Republic of China (Grant No. 2022YFA1402901), the Natural Science Foundation of Shaanxi Province (Grant No. 2023-JC-QN-0768), and the Natural Science Foundation of China (Grant No. 12074301).

- 
- \* zxguo08@xjtu.edu.cn
- <sup>1</sup> Z. Shen, S. Jing, Y. Heng, Y. Yao, K. N. Tu, and Y. Liu, *Appl. Phys. Rev.* **10**, 021309 (2023).
  - <sup>2</sup> H. Li, H. Jiang, Q. F. Sun, and X. C. Xie, [arXiv:2303.07692](https://arxiv.org/abs/2303.07692).
  - <sup>3</sup> S. A. Wolf, A. Y. Chtchelkanova, and D. M. Treger, *IBM J. Res. Dev.* **50**, 101 (2006).
  - <sup>4</sup> A. Avsar, H. Ochoa, F. Guinea, B. Özyilmaz, B. J. van Wees, and I. J. Vera-Marun, *Rev. Mod. Phys.* **92**, 021003 (2020).
  - <sup>5</sup> S. Sugahara and J. Nitta, Spin-transistor electronics: An overview and outlook, *Proc. IEEE* **98**, 2124 (2010).
  - <sup>6</sup> S. Datta and B. Das, Electronic analog of the electrooptic modulator, *Appl. Phys. Lett.* **56**, 665 (1990).
  - <sup>7</sup> B. Behin-Aein, D. Datta, S. Salahuddin, and S. Datta, *Nat. Nanotechnol.* **5**, 266 (2010).
  - <sup>8</sup> B. Dieny, I. L. Prejbeanu, K. Garello, P. Gambardella, P. Freitas, R. Lehdorff, W. Raberg, U. Ebels, S. O. Demokritov, and J. Akerman et al., *Nature Electronics* **3**, 446 (2020).
  - <sup>9</sup> G. F. A. Malik, M. A. Kharadi, F. A. Khanday, and N. Parveen, *Microelectron. J.* **106**, 104924 (2020).
  - <sup>10</sup> M. Rakibul Karim Akanda and R. K. Lake, *Appl. Phys. Lett.* **119**, 052402 (2021).
  - <sup>11</sup> L. Liang, Y. Yang, X. Wang, and X. Li, *Nano Lett.* **23**, 858 (2023).
  - <sup>12</sup> Y. Lu, R. Fei, X. Lu, L. Zhu, L. Wang, and L. Yang, *ACS Appl. Mater. Interfaces* **12**, 6243 (2020).
  - <sup>13</sup> L. Cao, X. Deng, G. Zhou, S. Liang, C. V. Nguyen, L. K. Ang, and Y. S. Ang, *Phys. Rev. B* **105**, 165302 (2022).
  - <sup>14</sup> G. Kresse and J. Furthmüller, *Phys. Rev. B* **54**, 11169 (1996).
  - <sup>15</sup> G. Kresse and J. Hafner, *Phys. Rev. B* **47**, 558 (1993).
  - <sup>16</sup> K. Wang, Y. Zhang, W. Zhao, P. Li, J. W. Ding, G. F. Xie, and Z. X. Guo, *Phys. Chem. Chem. Phys.* **21**, 9310 (2019).
  - <sup>17</sup> Z. X. Guo, Y. Y. Zhang, H. J. Xiang, X. G. Gong, and A. Oshiyama, *Phys. Rev. B* **92**, 201413(R) (2015).
  - <sup>18</sup> S. Smidstrup, T. Markussen, P. Vancaeyveld, J. Wellendorff, J. Schneider, T. Gunst, B. Verstichel, D. Stradi, P. A. Khomyakov, U. G. Vej-Hansen et al., *J. Phys.: Condens. Matter* **32**, 015901 (2020).
  - <sup>19</sup> J. Huang, P. Li, X. Ren, and Z. X. Guo, *Phys. Rev. Appl.* **16**, 044022 (2021).
  - <sup>20</sup> B. Liu, X. X. Ren, X. Zhang, P. Li, Y. Dong, Z. X. Guo, *Appl. Phys. Lett.* **122**, 152408 (2023).